Damping of climate-scale oceanic variability by mesoscale eddy turbulence

F. Sévellec*

Laboratoire d'Océanographie Physique et Spatiale, Univ-Brest CNRS IRD Ifremer, Brest, France

Ocean and Earth Science, University of Southampton, Southampton, UK

A. C. Naveira Garabato

Ocean and Earth Science, University of Southampton, Southampton, UK

T. Huck

Laboratoire d'Océanographie Physique et Spatiale, Univ-Brest CNRS IRD Ifremer, Brest, France

submitted to *Journal of Physical Oceanography*, 24 June 2020

revision 20 October 2020

* *Corresponding author address:* Laboratoire d'Océanographie Physique et Spatiale, Institut Universitaire Européen de la Mer, rue Dumont d'Urville, 29280 Plouzané, FRANCE. Phone: +33 290 91 5540 email: florian.sevellec@univ-brest.fr

Early Online Release: This preliminary version has been accepted for publication in *Journal of the Physical Oceanography*, may be fully cited, and has been assigned DOI 10.1175/JPO-D-20-0141.1. The final typeset copyedited article will replace the EOR at the above DOI when it is published.

Abstract

The impact of mesoscale eddy turbulence on long-term, climatic variability in the ocean's buoyancy structure is investigated using observations from a mooring deployed in the Drake Passage, Southern Ocean. By applying the Temporal-Residual-Mean framework and characterizing the variance contributors and the buoyancy variance budget, we identify the main source and sink of long-term buoyancy variance. Long-term buoyancy variance amplitude is set by long-term vertical velocity fluctuations acting on the steady stratification. This baroclinic buoyancy flux is also the main source of the variance, indicative of the effect of large-scale baroclinic instability. This source is balanced by a sink of long-term buoyancy variance associated with the vertical advection of the steady stratification by the eddy-induced circulation. We conclude that mesoscale eddy turbulence acts as a damping mechanism for long-term, climatic variability in the region of the observations, consistent with an 'eddy saturated' behaviour of the Antarctic Circumpolar Current.

Accepted for publication in *Journal of Physical Oceanography*. DOI 10.1175/JPO-D-20-0141.1.

1 Introduction

Mesoscale eddy turbulence is ubiquitous in the ocean (Wunsch, 2002; Chelton et al., 2007). It has long been hypothesized, and ultimately established, that this turbulence has significant impacts on the basin-scale ocean circulation, especially in the Southern Ocean (Gnanadesikan and Hallberg, 2000). While there is a vibrant discussion on the mechanistic nature of the eddies' role (Phillips and Rintoul, 2000; Hallberg and Gnanadesikan, 2001; Meredith and Hogg, 2006; Danabasoglu and Marshall, 2007; Smith and Gregory, 2009; Gent and Danabasoglu, 2011; Thompson and Naveira Garabato, 2014; Sinha and Abernathey, 2016; Marshall et al., 2017), it is now widely accepted that eddy turbulence is central to several fundamental features of the time-mean ocean circulation, such as the inter-basin meridional overturning (Nikurashin and Vallis, 2012). This has recently been corroborated in local observations in the Southern Ocean (Sévellec et al., 2019). However, no consensus exists on the eddies' effect on the ocean's climatic (i.e., interannual- and longer-time scale) variability (e.g., Huck et al., 2015; Sérazin et al., 2018), with eddies having been argued to either enhance or suppress such variability. Settling this debate is a foremost outstanding challenge of the climate science community.

The debate on the role of mesoscale eddy turbulence in modulating oceanic variability on climatic time scales entails two opposing views. On the one hand, several studies have shown that the transfer of surface kinetic energy (or of velocity variance) exhibits an inverse cascade (Arbic et al., 2014; Sérazin et al., 2015, 2018), implying that eddies are a source of long-term variability. On the other hand, mesoscale eddy turbulence is often represented as a sink of variance (Gent and McWilliams, 1990), whereby relatively small-scale baroclinic instability grows on a large-scale density front and induces a flattening of frontal isopycnals. The apparent discrepancy between these two views might stem from their adoption of fundamentally different approaches to describe the system, based on either the ocean's momentum budget (for the first view) or the buoyancy budget (for the second view), as suggested by

Accepted for publication in *Journal of Physical Oceanography*. DOI 10.1175/JPO-D-20-0141.1.

the pioneering work on oceanic turbulence of Rhines (1977) and Salmon (1978, 1980).

Despite its academic appearance, this debate has fundamental operational repercussions – for example, in the realm of interannual climate prediction. At present, climate projections are still provided by climate models incorporating eddy-less ocean models (i.e., ocean models where eddies are not resolved explicitly but only parameterized, Taylor et al., 2012). However, these models are seemingly too noisy to provide reliable interannual climate projections, an occurrence known as the signal-to-noise paradox of interannual climate prediction (Scaife and Smith, 2018; Sévellec and Drijfhout, 2019). This calls for clarification of the role of mesoscale eddy turbulence. Is it a further source of noise, degrading even more the reliability of interannual climate prediction? Or is it a damping mechanism, which needs to be accurately incorporated to improve predictive skill?

In this study, we directly assess the effect of eddies on the ocean's interannual variability by analysing measurements from a 2-year-long mooring deployment in a hotspot of eddy activity within the Antarctic Circumpolar Current (ACC). Our approach is based on the Temporal-Residual-Mean (TRM) framework (McDougall and McIntosh, 2001), and involves the formulation of the local buoyancy variance budget in a way that distinguishes between mesoscale eddy fluctuations and 'long-term' (i.e., with periods longer than those of eddies) variability. This enables us to quantify the intensity, and characterize the sources and sinks, of long-term buoyancy variance. We find that the main source of long-term buoyancy variance is the vertical advection of time-mean stratification by the fluctuating long-term circulation, whereas mesoscale eddies provide the primary sink of long-term buoyancy variance. Thus, we show that eddies suppress variations of the ACC density structure by restoring it to its mean state in the area of the observations.

The manuscript is organized as follows. The observational data are described in section 2. Section 3 presents our methodology, including the TRM framework, the calculation of vertical velocity with single-mooring measurements, and the formulation and implementation of the

Accepted for publication in *Journal of Physical Oceanography*. DOI 10.1175/JPO-D-20-0141.1.

buoyancy variance budget. Results are documented in section 4, and discussed in section 5. Conclusions are included within this last section.

2 Data

We analyse *in situ* observations acquired by a mooring deployed within the ACC, at 56°S, 57°50′W in the Drake Passage (Fig. 1a) under the auspices of the Diapycnal and Isopycnal Mixing Experiment in the Southern Ocean (DIMES, Naveira Garabato, 2010; Meredith, 2011). This location lies over a topographic feature and equatorward of the strongest ACC flow (for details of the exact location, see Brearley et al., 2013). The mooring considered here is the central mooring of the DIMES array, which was deployed for over 2 years between 12 December 2009 and 5 March 2012. The mooring contains conductivity-temperature-depth (CTD) instrumentation and current meters spanning the depth range between 1,200 m and 3,600 m, with a cluster around 2,000 m at a resolution of 100 m (Tab. 1). The observational data sets are those used in Brearley et al. (2013) and Sévellec et al. (2015, 2019), and a detailed quality control of the measurements is given in Brearley et al. (2013). The data are linearly interpolated onto constant pressure levels spaced by 100 dbar (other interpolating methods for mooring motion correction were tested, and found to induce quantitative changes in our diagnostics of less than 5%) with a temporal resolution of 15 minutes. We refer the reader to Sévellec et al. (2015) for a thorough estimation of measurement uncertainty. Finally, density and depth are computed using the Gibbs - SeaWater Oceanographic toolbox (McDougall and Barker, 2011).

From these observations, vertical velocities can be inferred, and the terms of a time-mean buoyancy budget can be diagnosed. The method to compute vertical velocities from single-mooring measurements is described in Sévellec et al. (2015); the mean statistical properties of the observational record are shown in Figs. 1b-g. Taking advantage of the equivalent-barotropic nature of the ACC flow (Killworth and Hughes, 2002), we define gradients in the

Accepted for publication in *Journal of Physical Oceanography*. DOI 10.1175/JPO-D-20-0141.1.

along and across directions of the time- and depth-mean flow (as indicated in Fig. 1a). This enables us to eliminate contributions to the buoyancy budget from the time-mean flow in the across direction (Fig. 1c), except for a small baroclinic component.

3 Method

a. Temporal-Residual-Mean framework

We formulate the buoyancy variance budget of the study area within the Temporal-Residual-Mean framework (McDougall and McIntosh, 2001). Starting from the evolution of buoyancy under negligible diffusion (Pe$\gg$1, where Pe is the Péclet number measuring the ratio of advection to diffusion), we have:

$$D_t b = 0, \tag{1}$$

where t is time, b is buoyancy, and D_t is the material derivative. This derivative can be expanded as $D_t{=}\partial_t{+}u\partial_x{+}v\partial_y{+}w\partial_z$, where x and y are the horizontal units for the along and across the time- and depth-mean flow directions, respectively; z is the vertical unit; u and v are the horizontal velocities for the along and across directions, respectively; and w is the vertical velocity.

To explicitly distinguish short-term (shorter than an arbitrary time scale τ) fluctuations from longer-term variability, we define $X{=}\bar{X}{+}X'$, where X represents any variable (e.g., b, u, v, or w), $\bar{X}(z,t){=}\int_{t-\frac{\tau}{2}}^{t+\frac{\tau}{2}} X(z,s)ds/\tau$ is the time-mean value of that variable at time t over the averaging time scale τ, and X' denotes the variable's temporal anomaly. Obviously, $\tau \leq (t_f - t_i)$, where t_i and t_f are the initial and final times, respectively, of the time series of X. From these definitions and following the TRM framework, we can transform (1) into

$$\hat{D}_t \hat{b} = 0, \tag{2}$$

where $\hat{D}_t$ is the TRM material derivative and $\hat{b}$ is the modified buoyancy. The TRM material derivative is given by $\hat{D}_t{=}\partial_t{+}\hat{u}\partial_x{+}\hat{v}\partial_y{+}\hat{w}\partial_z$, where $\hat{u}$ and $\hat{v}$ are the residual velocities for

Accepted for publication in *Journal of Physical Oceanography*. DOI 10.1175/JPO-D-20-0141.1.

the directions along and across the time- and depth-mean flow direction, respectively; and $\hat{w}$ is the residual vertical velocity. The modified buoyancy is $\hat{b}=\bar{b}+\tilde{b}$, where $\tilde{b}=-\partial_z(\bar{\phi}/\overline{N^2})$ is the re-scaled buoyancy variance with $\bar{\phi}=\overline{b'^2}/2$, and $N^2=\partial_z b$ is the squared Brunt-Väisälä frequency. The residual velocities are $\hat{u}=\bar{u}+\tilde{u}$, $\hat{v}=\bar{v}+\tilde{v}$, and $\hat{w}=\bar{w}+\tilde{w}$, where $\tilde{u}$ and $\tilde{v}$ are the eddy-induced velocities for the along and across directions, respectively; and $\tilde{w}$ is the eddy-induced vertical velocity. In the TRM framework, the horizontal eddy-induced velocities read

$$\tilde{u} = \partial_z \frac{-\overline{u'b'} + \frac{\bar{\phi}}{\overline{N^2}}\partial_z \bar{u}}{\overline{N^2}}, \tag{3a}$$

and

$$\tilde{v} = \partial_z \frac{-\overline{v'b'} + \frac{\bar{\phi}}{\overline{N^2}}\partial_z \bar{v}}{\overline{N^2}}. \tag{3b}$$

To avoid confusion with the classical TRM literature, it is important to note that we use different notations to, for instance, McDougall and McIntosh (2001). For the purpose of exactness, McDougall and McIntosh (2001) used different symbols to reflect the effects of different operators. Specifically, eddy-induced velocities and re-scaled buoyancy variance were expressed with distinct symbols in that work, since they were derived from two different operators. Here, without loss of accuracy, we choose a different approach. We refer to variables associated with eddy turbulent dynamics with a single symbol ($\tilde{}$), and to variables corrected from the eddy turbulent dynamics with a different symbol ($\hat{}$), regardless of the actual operators leading to each term. This allows for more compact, simplified formulations. Such an approach was already proposed in Sévellec et al. (2019), to which the present study is a natural follow-up.

To compute the variance of long-term fluctuations (i.e., fluctuations on time scales longer than τ), we can further decompose the time-averaged variables ($\hat{X}$) into steady ($\langle\hat{X}\rangle$) and fluctuating ($\hat{X}''$) components, such as $\hat{X}=\langle\hat{X}\rangle+\hat{X}''$, with $\langle\hat{X}\rangle(z)=\int_{t_i+\frac{\tau}{2}}^{t_f-\frac{\tau}{2}} \hat{X}(z,t)dt/(t_f-t_i-\tau)$. Using this time averaging, we can compute the temporal variance of the filtered modified buoyancy for different time filters, as $\sigma_\tau^2=\langle\hat{b}''^2\rangle$. Taking the derivative with respect to the

Accepted for publication in *Journal of Physical Oceanography*. DOI 10.1175/JPO-D-20-0141.1.

averaging time scale of this variance ($\partial_\tau \sigma_\tau^2$) yields the time-varying contribution of each time scale to the modified buoyancy variance (Fig. 2). This diagnostic shows that an important part of the modified buoyancy variance is contained in the super- and near-inertial regime (Fig. 2). However, although the contribution of this frequency range to variance is very high at any given time, its restricted spectral span (from 15 minutes to 1 day) makes it a negligible contributor to the total variance computed over the 2-year time scale of the observations. On this time scale, the dominant contribution to the variance is linked to the mesoscale eddy regime (1-100 days).

Having decomposed buoyancy into short-term fluctuations (b'), long-term fluctuations ($\hat{b}''$), and a steady component ($\langle \hat{b} \rangle$), we find that, while the steady component is independent of τ, the short- and long-term fluctuations obviously depend on τ. In the remainder of this work, we set τ to 100 days, so that short-term fluctuations correspond to mesoscale eddy motions, and long-term fluctuations correspond to longer-time scale variability, following our previous analysis of the buoyancy variance (Fig. 2) and recent works by Sévellec et al. (2015, 2019).

It is important to remind the reader that, despite the compact form of the equations within the TRM framework, as e.g., in (2), it remains possible to decompose all terms in order to trace back the individual contributions of short- or long-term fluctuations. We will subsequently take advantage of this property to assess the relative roles of short- and long-term fluctuations in determining the long-term buoyancy variance.

b. Computation of vertical velocity

To estimate the balances in (1)-(2), mooring measurements readily provide most of the needed quantities: $\partial_t b$, u, v, and $\partial_z b$. However, three required variables need to be estimated indirectly: $\partial_x b$, $\partial_y b$, and w. The horizontal buoyancy gradients are obtained using the three momentum equations, under the assumptions of low viscosity (Re$\gg$1), small inertial terms

Accepted for publication in *Journal of Physical Oceanography*. DOI 10.1175/JPO-D-20-0141.1.

(Ro$\ll$1) and hydrostatic balance. This set of equations reads

$$\partial_t u - fv = -\frac{1}{\rho_0}\partial_x P, \tag{4a}$$

$$\partial_t v + fu = -\frac{1}{\rho_0}\partial_y P, \tag{4b}$$

$$\partial_z P = \rho_0 b, \tag{4c}$$

where P is pressure; f is the Coriolis parameter; Re is the Reynolds number, which measures the ratio of inertial to viscous forces; and Ro is the Rossby number, which measures the ratio of inertial forces to the Coriolis acceleration. After algebraic manipulation, we obtain

$$\partial_x b = -\partial_t \partial_z u + f\partial_z v, \tag{5a}$$

$$\partial_y b = -\partial_t \partial_z v - f\partial_z u. \tag{5b}$$

Since u and v are known at all times and as a function of depth, both along and across buoyancy gradients can be evaluated from the mooring.

Finally, vertical velocity is obtained with (1) and (5), such as:

$$w = -\frac{\partial_t b}{N^2} + \frac{f}{N^2}\left(v\partial_z u - u\partial_z v\right) + \frac{1}{N^2}\left(u\partial_t\partial_z u + v\partial_t\partial_z v\right). \tag{6}$$

This method closely follows the study of Sévellec et al. (2015), to which we refer the reader for further details. Sévellec et al. (2015) demonstrate the validity of the assumptions adopted here (in particular, Ro$\ll$1 along the vertical), and the consistency of the leading-order balance of the equations with quasi-geostrophy, which is a widely used approximation in studying mesoscale turbulence. Errors in derived variables were also estimated by those authors, and confirm the accuracy of the method.

Following the same logic, the eddy-induced vertical velocity can be diagnosed using (2), following Sévellec et al. (2019), as:

$$\tilde{w} = -\overline{w} - \frac{\partial_t \hat{b}}{\hat{N}^2} - \frac{\hat{u}\partial_x \hat{b} + \hat{v}\partial_y \hat{b}}{\hat{N}^2}, \tag{7}$$

where $\hat{N}^2{=}\partial_z \hat{b}$ is the modified stratification.

Accepted for publication in *Journal of Physical Oceanography*. DOI 10.1175/JPO-D-20-0141.1.

c. Buoyancy variance budget and contributors

Now that the modified buoyancy and residual velocities have been defined, we can look at their temporal evolution across the 2-year mooring record, at all depths (Fig. 3). All the time series display substantial variations. For the buoyancy, these variations are intensified in the upper part of the mooring, between 1,200 m and 1,800 m, and decrease with depth with the same sign signature over the vertical. This is expected from the equivalent-barotropic structure of the ACC flow (Killworth and Hughes, 2002). For the horizontal velocities, variations peak at 10 cm s^{-1}, a value comparable to the time-mean velocities. In relative terms, variations are stronger for the across velocities (with frequent sign reversals) than for the along velocities. For the vertical velocities, variations peak around 0.5 mm s^{-1}, and are intensified around 2,000 m with opposing velocities above and below this depth.

Since all aspects of buoyancy variability can be determined from a single mooring, we re-visit (2) with the aim of identifying the sources and sinks of such variability. With this purpose, we apply a Reynolds decomposition using an Eulerian time averaging. We decompose all terms into steady ($\langle \hat{X} \rangle$) and fluctuating ($\hat{X}''$) components, and find that the steady component is controlled by the equation:

$$\begin{aligned} \partial_t \langle \hat{b} \rangle \;\; &+ \;\; \langle \hat{u} \rangle \, \partial_x \langle \hat{b} \rangle + \langle \hat{v} \rangle \, \partial_y \langle \hat{b} \rangle + \langle \hat{w} \rangle \, \partial_z \langle \hat{b} \rangle \\ &= \;\; - \langle \hat{u}'' \partial_x \hat{b}'' \rangle - \langle \hat{v}'' \partial_y \hat{b}'' \rangle - \langle \hat{w}'' \partial_z \hat{b}'' \rangle \, . \end{aligned} \tag{8}$$

This form of the mean buoyancy balance was applied and examined by Sévellec et al. (2019). We next exploit this relation to formulate the buoyancy variance budget.

Accepted for publication in *Journal of Physical Oceanography*. DOI 10.1175/JPO-D-20-0141.1.

1) Buoyancy Variance Budget

From (2) and (8), we can express the temporal evolution of the long-term fluctuations of buoyancy as

$$\begin{aligned} \partial_t \hat{b}'' &+ \langle \hat{u} \rangle \partial_x \hat{b}'' + \langle \hat{v} \rangle \partial_y \hat{b}'' + \langle \hat{w} \rangle \partial_z \hat{b}'' + \hat{u}'' \partial_x \langle \hat{b} \rangle + \hat{v}'' \partial_y \langle \hat{b} \rangle + \hat{w}'' \partial_z \langle \hat{b} \rangle \\ &= -\hat{u}'' \partial_x \hat{b}'' - \hat{v}'' \partial_y \hat{b}'' - \hat{w}'' \partial_z \hat{b}'' + \langle \hat{u}'' \partial_x \hat{b}'' \rangle + \langle \hat{v}'' \partial_y \hat{b}'' \rangle + \langle \hat{w}'' \partial_z \hat{b}'' \rangle \,. \end{aligned} \tag{9}$$

Multiplying this equation by $2\hat{b}''$, we derive the time-evolving budget of long-term buoyancy variance estimated from low-pass filtered residual fields

$$\begin{aligned} \langle \partial_t \hat{b}''^2 \rangle &= -2 \langle \hat{u} \rangle \langle \hat{b}'' \partial_x \hat{b}'' \rangle - 2 \langle \hat{v} \rangle \langle \hat{b}'' \partial_y \hat{b}'' \rangle - 2 \langle \hat{w} \rangle \langle \hat{b}'' \partial_y \hat{b}'' \rangle \\ &\quad -2 \langle \hat{u}'' \hat{b}'' \rangle \langle \partial_x \hat{b} \rangle - 2 \langle \hat{v}'' \hat{b}'' \rangle \langle \partial_y \hat{b} \rangle - 2 \langle \hat{w}'' \hat{b}'' \rangle \langle \partial_z \hat{b} \rangle \\ &\quad -2 \langle \hat{u}'' \hat{b}'' \partial_x \hat{b}'' \rangle - 2 \langle \hat{v}'' \hat{b}'' \partial_y \hat{b}'' \rangle - 2 \langle \hat{w}'' \hat{b}'' \partial_z \hat{b}'' \rangle \,. \end{aligned} \tag{10}$$

The budget of long-term buoyancy variance is found to be controlled by three components: the steady velocity term (Bud-SV, corresponding to the right hand side of the first line), the steady buoyancy term (Bud-SB, corresponding to the second line), and the turbulent long-term fluctuation term (Bud-TL, corresponding to the third line). Each component can be further decomposed into contributions from each of the three directions (along, across, and vertical), such as e.g., Bud-SV=Bud-SV$_x$+Bud-SV$_y$+Bud-SV$_z$. The time-evolving form of the buoyancy variance budget synthesized in (10) will be especially useful in determining sources and sinks of long-term buoyancy variance. This method of computing the buoyancy variance budget has been applied in a range of studies to describe oceanic variability (Sévellec et al., 2006; Arzel et al., 2006; Buckley et al., 2012).

2) Buoyancy Variance Contributors

In order to determine the overall (i.e., integrated over the entire mooring record) contributors to long-term buoyancy variance, we integrate (9) with respect to time, and obtain the

Accepted for publication in *Journal of Physical Oceanography*. DOI 10.1175/JPO-D-20-0141.1.

following expression for the long-term fluctuations of modified buoyancy:

$$\begin{aligned}
\hat{b}'' = \hat{b}''\Big|_{t_1} \quad &- \int_{t_1}^{t} \langle \hat{u} \rangle \, \partial_x \hat{b}'' ds - \int_{t_1}^{t} \langle \hat{v} \rangle \, \partial_y \hat{b}'' ds - \int_{t_1}^{t} \langle \hat{w} \rangle \, \partial_z \hat{b}'' ds \\
&- \int_{t_1}^{t} \hat{u}'' \partial_x \langle \hat{b} \rangle \, ds - \int_{t_1}^{t} \hat{v}'' \partial_y \langle \hat{b} \rangle \, ds - \int_{t_1}^{t} \hat{w}'' \partial_z \langle \hat{b} \rangle \, ds \\
&- \int_{t_1}^{t} \hat{u}'' \partial_x \hat{b}'' ds - \int_{t_1}^{t} \hat{v}'' \partial_y \hat{b}'' ds - \int_{t_1}^{t} \hat{w}'' \partial_z \hat{b}'' ds \\
&+ \left(\langle \hat{u}'' \partial_x \hat{b}'' \rangle + \langle \hat{v}'' \partial_y \hat{b}'' \rangle + \langle \hat{w}'' \partial_z \hat{b}'' \rangle \right) (t - t_1) \\
&+ \left(\langle \overline{u' \partial_x b'} \rangle + \langle \overline{v' \partial_y b'} \rangle + \langle \overline{w' \partial_z b'} \rangle \right) (t - t_1) \, . \qquad (11)
\end{aligned}$$

Multiplying this equation by $\hat{b}''$, we derive a decomposition of the long-term buoyancy variance within the TRM framework in terms of its contributors:

$$\begin{aligned}
\langle \hat{b}''^2 \rangle \quad = \quad &- \langle \hat{u} \rangle \langle \hat{b}'' \int_{t_1}^{t} \partial_x \hat{b}'' ds \rangle - \langle \hat{v} \rangle \langle \hat{b}'' \int_{t_1}^{t} \partial_y \hat{b}'' ds \rangle - \langle \hat{w} \rangle \langle \hat{b}'' \int_{t_1}^{t} \partial_z \hat{b}'' ds \rangle \\
&- \langle \hat{b}'' \int_{t_1}^{t} \hat{u}'' ds \rangle \, \partial_x \langle \hat{b} \rangle - \langle \hat{b}'' \int_{t_1}^{t} \hat{v}'' ds \rangle \, \partial_y \langle \hat{b} \rangle - \langle \hat{b}'' \int_{t_1}^{t} \hat{w}'' ds \rangle \, \partial_z \langle \hat{b} \rangle \\
&- \langle \hat{b}'' \int_{t_1}^{t} \hat{u}'' \partial_x \hat{b}'' ds \rangle - \langle \hat{b}'' \int_{t_1}^{t} \hat{v}'' \partial_y \hat{b}'' ds \rangle - \langle \hat{b}'' \int_{t_1}^{t} \hat{w}'' \partial_z \hat{b}'' ds \rangle \\
&+ \left(\langle \hat{u}'' \partial_x \hat{b}'' \rangle + \langle \hat{v}'' \partial_y \hat{b}'' \rangle + \langle \hat{w}'' \partial_z \hat{b}'' \rangle \right) \langle \hat{b}'' t \rangle \, . \qquad (12)
\end{aligned}$$

Following the decomposition principle used for the time-evolving budget of long-term buoyancy variance in (10), we define three distinct contributors: the steady velocity term (Var-SV, corresponding to the right hand side of the first line), the steady buoyancy term (Var-SB, corresponding to the second line), and the turbulent long-term fluctuation term (Var-TL, corresponding to the third and fourth lines). Also, as before, each component is further decomposed into contributions from each of the three directions, such as e.g., Var-SV=Var-SV_x+Var-SV_y+Var-SV_z.

4 Results

The first important result of our TRM framework-based analysis of the long-term buoyancy variance is that both the time-evolving variance budget and the decomposition into overall

Accepted for publication in *Journal of Physical Oceanography*. DOI 10.1175/JPO-D-20-0141.1.

variance contributors [given by (10) and (12), respectively] have negligible closure errors (Fig. 4). This endorses the robustness of our proposed formulations of the variance budget and of the variance contributors, and their subsequent application to the mooring data.

The long-term buoyancy variance contributor analysis (Fig. 5) shows that the two most important terms at all depths are the along advection of long-term buoyancy fluctuations by the steady velocity (Var-SV$_x$) and the across advection of steady buoyancy by long-term velocity fluctuations (Var-SB$_y$). The Var-SV$_x$ term makes a positive contribution to the total variance, whereas the Var-SB$_y$ term makes a negative contribution. The two terms compensate one another almost perfectly, and thereby exert a negligible joint impact on the long-term buoyancy variance. This result is consistent with the non-Doppler-shifted effect expected from the passage of large-scale Rossby waves (Rossby et al., 1939; Held, 1983; Killworth et al., 1997; Sévellec and Fedorov, 2013), a phenomenon that has been extensively documented in the Southern Ocean. Invoking geostrophic balance to relate $\langle \bar{u} \rangle$ to $\partial_y \langle \bar{b} \rangle$ and $\bar{v}''$ to $\partial_x \bar{b}''$, we infer that the advection of the anomalous buoyancy by the mean along velocity ($\langle \bar{u} \rangle \, \partial_x \bar{b}''$, controlling Var-SV$_x$) and the advection of mean buoyancy by the anomalous across velocity ($\bar{v}'' \partial_y \langle \bar{b} \rangle$, controlling Var-SB$_y$) balance each other almost perfectly. Thus, as a result of this compensation between Var-SV$_x$ and Var-SB$_y$, we find that long-term buoyancy variance is primarily controlled by the vertical advection of steady buoyancy by long-term velocity fluctuations (Var-SB$_z$), again in accord with large-scale Rossby wave dynamics. It is interesting to note that neither the long-term nor the short-term turbulent components (not shown) contribute to setting the long-term buoyancy variance. This suggests, in other words, that mesoscale eddies do not directly affect the amplitude of the long-term buoyancy variance. This also reinforces the validity of the non-Doppler-shifted effect, where mesoscale eddy turbulent fluxes were ignored. [Note, however, that eddies do contribute to determining the steady components (Sévellec et al., 2019), and so indirectly contribute to setting the amplitude of the long-term buoyancy variance.]

Accepted for publication in *Journal of Physical Oceanography*. DOI 10.1175/JPO-D-20-0141.1.

The time-evolving budget of long-term buoyancy variance, which allows us to distinguish between sources and sinks of variance (Fig. 6), shows that the main balance is established between three terms: the along advection of long-term buoyancy fluctuations by the steady flow (Bud-SV$_x$), the across advection of steady stratification by long-term velocity fluctuations (Bud-SB$_y$), and the vertical advection of steady stratification by long-term velocity fluctuations (Bud-SB$_z$). This indicates that Bud-SV$_x$ and Bud-SB$_y$ act as upper and deeper sources of long-term buoyancy variance, respectively, whereas Bud-SB$_z$ provides a sink.

We may now effect a further decomposition of these three leading terms, in order to evaluate the role of short-term mesoscale eddy turbulence in energising or damping long-term buoyancy variance. With this purpose, we exploit a convenient property of the TRM framework, within which the respective roles of short- and long-term fluctuations can be traced back by splitting the modified buoyancy into the Eulerian time-mean buoyancy and the re-scaled buoyancy variance, and by partitioning the residual velocities into the Eulerian time-mean velocities and the eddy-induced velocities (as defined in section 3a.). This decomposition reads:

$$\begin{aligned}
\text{Bud-SV}_x &= -2\,\langle \hat{u} \rangle\, \langle \hat{b}''\partial_x \hat{b}'' \rangle\,, \\
&= -2\,\langle \hat{u} \rangle \left[\langle \bar{b}''\partial_x \bar{b}'' \rangle + \langle \bar{b}''\partial_x \tilde{b}'' \rangle + \langle \tilde{b}''\partial_x \bar{b}'' \rangle + \langle \tilde{b}''\partial_x \tilde{b}'' \rangle \right], \\
&= \mathrm{B_L}\Delta_\mathrm{L} + \mathrm{B_L}\Delta_\mathrm{S} + \mathrm{B_S}\Delta_\mathrm{L} + \mathrm{B_S}\Delta_\mathrm{S}, \qquad (13a)
\end{aligned}$$

$$\begin{aligned}
\text{Bud-SB}_y &= -2\,\langle \hat{v}''\hat{b}'' \rangle\, \langle \partial_y \hat{b} \rangle\,, \\
&= -2 \left[\langle \bar{v}''\bar{b}'' \rangle + \langle \bar{v}''\tilde{b}'' \rangle + \langle \tilde{v}''\bar{b}'' \rangle + \langle \tilde{v}''\tilde{b}'' \rangle \right] \langle \partial_y \hat{b} \rangle\,, \\
&= \mathrm{V_L B_L} + \mathrm{V_L B_S} + \mathrm{V_S B_L} + \mathrm{V_S B_S}, \qquad (13b)
\end{aligned}$$

Accepted for publication in *Journal of Physical Oceanography*. DOI 10.1175/JPO-D-20-0141.1.

and

$$\begin{aligned}
\text{Bud-SB}_z &= -2\left\langle \hat{w}''\hat{b}''\right\rangle \left\langle \partial_z \hat{b}\right\rangle, \\
&= -2\left[\left\langle \bar{w}''\bar{b}''\right\rangle + \left\langle \bar{w}''\tilde{b}''\right\rangle + \left\langle \tilde{w}''\bar{b}''\right\rangle + \left\langle \tilde{w}''\tilde{b}''\right\rangle\right]\left\langle \partial_z \hat{b}\right\rangle, \\
&= \text{W}_\text{L}\text{B}_\text{L} + \text{W}_\text{L}\text{B}_\text{S} + \text{W}_\text{S}\text{B}_\text{L} + \text{W}_\text{S}\text{B}_\text{S}. \qquad (13c)
\end{aligned}$$

Applying this decomposition to our data (Fig. 7) reveals that, while all terms within Bud-SV$_x$ and Bud-SB$_y$ (the sources of long-term buoyancy variance) are modest in comparison with Bud-SV$_x$ and Bud-SB$_y$, respectively, the components of Bud-SB$_z$ (the sink of long-term buoyancy variance) can be as much as 4 times larger than Bud-SB$_z$ (or Bud-SV$_x$ and Bud-SB$_y$) and of opposite signs. This result indicates that the time-evolving budget of long-term buoyancy variance is primarily controlled by a balance concealed within Bud-SB$_z$. In this balance, long-term buoyancy variance is generated by the vertical advection of the steady stratification by long-term velocity fluctuations (i.e., positive $-2\left\langle \bar{w}''\bar{b}''\right\rangle \left\langle \partial_z \hat{b}\right\rangle$), and is damped by the vertical advection of the steady stratification by short-term velocity fluctuations (i.e., negative $-2\left\langle \tilde{w}''\bar{b}''\right\rangle \left\langle \partial_z \hat{b}\right\rangle$). Thus, our analysis of the observations shows that short-term mesoscale eddy turbulence suppresses long-term buoyancy variability in the study area, rather than stimulating such variability as an internal noise source as is often hypothesized. This finding is consistent with eddy turbulence closures following Gent and McWilliams (1990), which act to dampen buoyancy variance. Moreover, $\left\langle \bar{w}''\bar{b}''\right\rangle$ and $\left\langle \tilde{w}''\tilde{b}''\right\rangle$ are the baroclinic flux by the long-term fluctuations and the baroclinic eddy flux, respectively, and act as a baroclinic conversion between eddy potential energy and eddy kinetic energy, consistent with the occurrence of baroclinic instability (Harrison et al., 1978; Marchesiello et al., 2003).

To conclude, it is interesting to note that a buoyancy variance budget of the short-term buoyancy variance (not shown) reveals that the main sink of long-term buoyancy variance

Accepted for publication in *Journal of Physical Oceanography*. DOI 10.1175/JPO-D-20-0141.1.

becomes the main source of short-term buoyancy variance. This illustrates that mesoscale eddy turbulence is sustained by short-term vertical advection of the steady stratification, consistently with small-scale baroclinic instability and the Gent and McWilliams (1990) eddy turbulent closure. It is also worth noting than the variance budget computed in the traditional Eulerian framework suggests that the mesoscale eddy turbulence is damping the long-term fluctuations too. The damping occurs through the horizontal buoyancy flux, however. This demonstrates the usefulness of the TRM framework to account for vertical buoyancy flux compensation (by accurately re-distributing the turbulent fluxes), and the overall robustness of the results.

5 Conclusion

Oceanic variability on interannual and longer time scales has been established to play an important role in shaping regional and global climate (Watanabe et al., 2013; Haarsma et al., 2016). Observational snapshots of the ocean, however, are mainly characterized by mesoscale eddy turbulence acting on shorter time scales of days to months (Wunsch, 2002; Chelton et al., 2007). A significant outstanding challenge in physical oceanography and climate science is to reconcile these two disparate views of oceanic variability, by assessing the effect of mesoscale eddy turbulence on longer-term, climatic changes in the ocean. This question has hitherto been addressed in two ways, with contrasting results. On the one hand, several studies (largely based on the analysis of numerical models) have considered spectral surface kinetic energy transfers occurring within the ocean circulation to suggest the existence of an inverse cascade, via which mesoscale eddy turbulence energises motions on longer time scales (e.g., Arbic et al., 2014; Sérazin et al., 2015, 2018). The occurrence of this inverse kinetic energy cascade is interpreted to signify that mesoscale eddies act as a source of oceanic climate variability. On the other hand, a range of theoretical and numerical investigations propose that long-term oceanic variability is instead sourced from a large-scale baroclinic

Accepted for publication in *Journal of Physical Oceanography*. DOI 10.1175/JPO-D-20-0141.1.

instability that draws energy from the mean state (Colin de Verdière and Huck, 1999; Huck and Vallis, 2001; Sévellec and Huck, 2015; Hochet et al., 2020), and that mesoscale eddies provide a damping mechanism for the variability. In the present work, we have attempted to shed light on this debate by putting forward a new, observationally grounded perspective, entailing the computation of the budget of long-term buoyancy variance within the TRM framework from mooring measurements in a Southern Ocean mesoscale eddy hotspot.

Our analysis shows that the buoyancy variance in the study area is dominated ($\sim$80% of the total variance) by features acting on time scales between $2\pi/f$ and ~ 100 days, associated with mesoscale eddy turbulence as determined by previous studies (Sévellec et al., 2015, 2019). Although super-inertial buoyancy variability is large, its restricted spectral footprint makes its contribution negligible to the total buoyancy variance. Long-term variability (on time scales longer than 100 days) is also notable, and contributes between 15 and 20% of the total buoyancy variance.

Decomposing the long-term buoyancy variance into its distinct contributors reveals that long-term variability is predominantly induced by the along advection of long-term buoyancy fluctuations by the steady ocean circulation and by the across advection of steady buoyancy by long-term velocity fluctuations. There is, however, substantial cancellation between these two contributors, consistent with the non-Doppler-shifted effect expected from the passage of large-scale Rossby waves (Rossby et al., 1939; Held, 1983; Killworth et al., 1997; Sévellec and Fedorov, 2013). As a result, long-term buoyancy variance primarily results from the vertical advection of the steady stratification by long-term velocity fluctuations.

Examination of the time-evolving budget of long-term buoyancy variance reveals the sources and sinks of long-term variability. Unlike in the case of kinetic energy (i.e., momentum variance) considered by previous studies (e.g., Arbic et al., 2014; Sérazin et al., 2015, 2018), mesoscale eddies are found to dampen long-term variability (consistenty with recent numerical simulations of Hochet et al., 2020). This sink is balanced by a source of long-

Accepted for publication in *Journal of Physical Oceanography*. DOI 10.1175/JPO-D-20-0141.1.

term buoyancy variance effected by long-term vertical velocity fluctuations acting on the steady stratification, as expected from large-scale baroclinic instability (Colin de Verdière and Huck, 1999; Sévellec and Huck, 2015). The obvious difference between these two views is their depth of applicability: at surface for the kinetic energy-based view, and at sub-surface for the buoyancy variance-based view. Such consideration aside, these views' discrepancy on the expected impact of mesoscale eddies on oceanic climate variability suggests that the variances of horizontal velocities and of buoyancy behave in contrasting ways. A possible rationalization of this result is that, as kinetic energy is transferred to longer time scales, it energizes motions of increasingly larger horizontal scales (e.g., Arbic et al., 2014). Through geostrophy, this implies that the buoyancy anomalies associated with eddies will be distributed over increasing horizontal scales too, such that the local amplitude of the anomalies will decrease as eddies grow (in both size and period). This is likely to result in eddies acting as a sink of long-term buoyancy variance. Note, however, that this apparent paradox is a classical result of quasi-geostrophic turbulence, as discussed in the works of Rhines (1977) and Salmon (1978, 1980). In this context, kinetic energy exhibits an inverse cascade, whereas potential energy undergoes a forward cascade. Our results provide observational evidence for this predicted behavior of oceanic turbulence.

Our budget of long-term buoyancy variance indicates that a leading-order balance is established between a source and a sink underpinned by vertical flow (i.e., long-term fluctuations in the vertical buoyancy flux balanced by the eddy-induced vertical buoyancy flux). Thus, within the TRM formalism, there is no net source or sink of long-term buoyancy variance in our observations. This result is consistent with the eddy turbulent closures based on Gent and McWilliams (1990), which have been shown to adequately represent the mean state of the study area (Sévellec et al., 2019). This overall compensation suggests the implicit action of the eddy turbulence flux (i.e., only balancing the Eulerian mean); it would thus be interesting to diagnose its explicit impact through the momentum balance (i.e., acting as an

Accepted for publication in *Journal of Physical Oceanography*. DOI 10.1175/JPO-D-20-0141.1.

extra stress, McDougall and McIntosh, 2001).

Further, our diagnostics provide direct observational evidence of the 'eddy-saturated' behaviour of the ACC (Thompson and Naveira Garabato, 2014; Hallberg and Gnanadesikan, 2001; Meredith and Hogg, 2006; Gent and Danabasoglu, 2011; Sinha and Abernathey, 2016; Marshall et al., 2017), by showing that long-term changes in the ACC's that long-terms changes in the density structure, induced (commonly by wind forcing) via a perturbed vertical buoyancy flux, are relaxed toward equilibrium via the damping action of eddies. More generally, our findings suggest that mesoscale eddy turbulence might suppress, or contribute to suppress, the signal-to-noise paradox (Scaife and Smith, 2018; Sévellec and Drijfhout, 2019) of interannual climate prediction by removing or alleviating the level of noise in climate models.

While we believe that our study offers a significant contribution to the discussion on the impact of mesoscale eddy turbulence on oceanic climate variability, this contribution comes with some caveats. Chief amongst these is the possibly rather unusual dynamics of our study area, which is characterized by intense eddy activity and so is not necessarily representative of the wider Southern Ocean or, for that matter, other regions in the global ocean. A further shortcoming of our work is its reliance on a single mooring, which limits the geographical scope of our analysis. Both of these caveats call for an application of the analytical approach put forward here to mooring observations elsewhere, and to eddy-permitting and -resolving numerical models. This will be the goal of a follow-up study.

Our results indicate that mesoscale eddy turbulence exerts a stabilizing effect on oceanic climate variability. The question remains, however, of how this stabilizing role impacts the occurrence of basin-scale modes of climate variability, such as the Atlantic Multidecadal Variability (e.g., Kushnir, 1994). Indeed, this question is the subject of an ongoing debate, whereby one school of thought (LaCasce and Pedlosky, 2004) suggests that mesoscale eddy damping inhibits the existence of basin-scale climatic modes; and another (Sévellec and Huck,

Accepted for publication in *Journal of Physical Oceanography*. DOI 10.1175/JPO-D-20-0141.1.

2015) proposes that the damping acts as a selector of unstable basin-scale climatic modes. This latter hypothesis is supported by eddy-permitting simulations, which have been shown to contain basin-scale climatic modes (Huck et al., 2015; Hochet et al., 2020). However, the debate remains unaddressed from an observational angle. Tackling this gap will be the aim of future work.

Acknowledgment. This research was supported by the UK Natural and Environmental Research Council (SMURPHS, NE/N005767/1 to FS and DIMES, NE/F020252/1 to ACNG) and by the DECLIC project funded through the French CNRS/INSU/LEFE program. ACNG acknowledges the support of the Royal Society and the Wolfson Foundation This work was supported by ISblue project, Interdisciplinary graduate school for the blue planet (ANR-17-EURE-0015) and co-funded by a grant from the French government under the program "Investissements d'Avenir".

Accepted for publication in *Journal of Physical Oceanography*. DOI 10.1175/JPO-D-20-0141.1.

References

Arbic, B. K., et al., 2014: Geostrophic turbulence in the frequency-wavenumber domain: Eddy-driven low-frequency variability. *J. Phys. Oceanogr.*, **44**, 2050–2069.

Arzel, O., T. Huck, and A. Colin de Verdière, 2006: The different nature of the interdecadal variability of the thermohaline circulation under mixed and flux boundary conditions. *J. Phys. Oceanogr.*, **36**, 1703–1718.

Brearley, J. A., et al., 2013: Eddy-induced modulation of turbulent dissipation over rough topography in the Southern Ocean. *J. Phys. Oceanogr.*, **43**, 2288–2308.

Buckley, M. W., et al., 2012: On the relationship between decadal buoyancy anomalies and variability of the Atlantic meridional overturning circulation. *J. Climate*, **25**, 8009–8030.

Chelton, D. B., et al., 2007: Global observations of large oceanic eddies. *Geophys. Res. Lett.*, **34**, L15 606.

Colin de Verdière, A. and T. Huck, 1999: Baroclinic instability: an oceanic wavemaker for interdecadal variability. *J. Phys. Oceanogr.*, **29**, 893–910.

Danabasoglu, G. and J. Marshall, 2007: Effects of vertical variations of thickness diffusivity in an ocean general circulation model. *Ocean Modell.*, **18**, 122–141.

Gent, P. R. and G. Danabasoglu, 2011: Response to Increasing Southern Hemisphere Winds in CCSM4. *J. Climate*, **24**, 4992–4998.

Gent, P. R. and J. C. McWilliams, 1990: Isopycnal mixing in ocean circulation model. *J. Phys. Oceanogr.*, **20**, 150–155.

Gnanadesikan, A. and R. Hallberg, 2000: On the Relationship of the Circumpolar Current to Southern Hemisphere Winds in Coarse-Resolution Ocean Models. *J. Phys. Oceanogr.*, **30**, 2013–2034.

Accepted for publication in *Journal of Physical Oceanography*. DOI 10.1175/JPO-D-20-0141.1.

Haarsma, R. J., F. M. Selten, and S. S. Drijfhout, 2016: Decelerating Atlantic meridional overturning circulation main cause of future west European summer atmospheric circulation changes. *Environ. Res. Lett.*, **10**, 094 007.

Hallberg, R. and A. Gnanadesikan, 2001: An Exploration of the Role of Transient Eddies in Determining the Transport of a Zonally Reentrant Current. *J. Phys. Oceanogr.*, **31**, 3312–3330.

Harrison, D., E. and A. R. Robison, 1978: Energy analysis of open regions of turbulent flows: mean eddy energetics of a numerical ocean circulation experiment. *Dyn. Atmos. Oceans*, **2**, 185–211.

Held, I. M., 1983: *Stationary and quasi-stationary eddies in the extratropical troposphere: Theory*. Large-Scale Dynamical Processes in the Atmosphere, B. J. Hoskins, and R. P. Pearce, Eds., Academic Press, pp. 127–168.

Hochet, A., et al., 2020: Direct temporal cascade of temperature variance in eddy-permitting simulations of multidecadal variability. *J. Climate*, **33**, 9409–9425.

Huck, T., O. Arzel, and F. Sévellec, 2015: Multidecadal variability of the overturning circulation in presence of eddy turbulence. *J. Phys. Oceanogr.*, **45**, 157–173.

Huck, T. and G. K. Vallis, 2001: Linear stability analysis of three-dimensional thermally-driven ocean circulation: application to interdecadal oscillations. *Tellus*, **53A**, 526–545.

Killworth, P. D., D. B. Chelton, and R. A. de Szoeke, 1997: The speed of observed and theoretical long extratropical planetary waves. *J. Phys. Oceanogr.*, **27**, 1946–1966.

Killworth, P. D. and C. W. Hughes, 2002: The Antarctic Circumpolar Current as a free equivalent-barotropic jet. *J. Mar. Res.*, **60**, 19–45.

Accepted for publication in *Journal of Physical Oceanography*. DOI 10.1175/JPO-D-20-0141.1.

Kushnir, Y., 1994: Interdecadal variations in North Atlantic sea surface temperature and associated atmospheric conditions. *J. Climate*, **7**, 141–157.

LaCasce, J. H. and J. Pedlosky, 2004: The instability of Rossby basin modes and the oceanic eddy field. *J. Phys. Oceanogr.*, **34**, 2027–2041.

Marchesiello, P., J. C. McWilliams, and A. Shchepetkin, 2003: Equilibrium Structure and Dynamics of the California Current System. *J. Phys. Oceanogr.*, **33**, 753–783.

Marshall, D. P., et al., 2017: Eddy saturation and frictional control of the Antarctic Circumpolar Current. *Geophys. Res. Lett.*, **44**, 286–292.

Maximenko, N., et al., 2009: Mean dynamic topography of the ocean derived from satellite and drifting buoy data using three different techniquesP. *J. Atmos. Oceanic Tech.*, **26**, 1910–1919.

McDougall, T. J. and P. M. Barker, 2011: Getting started with TEOS-10 and the Gibbs Seawater (GSW) Oceanographic Toolbox. Tech. rep., SCOR/IAPSO WG127.

McDougall, T. J. and P. C. McIntosh, 2001: The Temporal-Residual-Mean Velocity. Part II: Isopycnal Interpretation and the Tracer and Momentum Equations. *J. Phys. Oceanogr.*, **31**, 1222–1246.

Meredith, M. P., 2011: Cruise report: RRS James Cook JC054 (DIMES UK2) 30 Nov 2010 to 8 Jan 2011. Tech. rep., British Antarctic Survey Cruise Rep. 206pp.

Meredith, M. P. and A. M. Hogg, 2006: Circumpolar response of Southern Ocean eddy activity to a change in the Southern Annular Mode. *Geophys. Res. Lett.*, **33**, L16 608.

Naveira Garabato, A. C., 2010: Cruise Report RRS James Cook JC041 (DIMES UK1) 5 Dec 2009 to 21 Dec 2009. Tech. rep., National Oceanography Centre Southampton Cruise Rep. 164pp.

Accepted for publication in *Journal of Physical Oceanography*. DOI 10.1175/JPO-D-20-0141.1.

Nikurashin, M. and G. Vallis, 2012: A Theory of the Interhemispheric Meridional Overturning Circulation and Associated Stratification. *J. Phys. Oceanogr.*, **42**, 1652–1667.

Phillips, H. E. and S. R. Rintoul, 2000: Eddy Variability and Energetics from Direct Current Measurements in the Antarctic Circumpolar Current South of Australia. *J. Phys. Oceanogr.*, **30**, 3050–3076.

Rhines, P. B., 1977: The Dynamics of Unsteady Currents. *The Sea*, **Vol. VI**, John Wiley and Sons, New York.

Rossby, C. G. et al., 1939: Relation between variations in the intensity of the zonal circulation of the atmosphere and the displacements of the semi-permanent centers of action. *J. Mar. Res.*, **2**, 38–55.

Salmon, R. B., 1978: Two-layer quasi-geostrophic turbulence in a simple special case. *Geophys. Astrophys. Fluid Dyn.*, **10**, 25–52.

—, 1980: Baroclinic instability and geostrophic turbulence. *Geophys. Astrophys. Fluid Dyn.*, **10**, 167–211.

Scaife, A. A. and D. Smith, 2018: A signal-to-noise paradox in climate science. *npj Climate and Atmospheric Science*, **1**, 28.

Sérazin, G., et al., 2015: Intrinsic variability of sea level from global ocean simulations: Spatiotemporal scales. *J. Climate*, **28**, 4279–4292.

—, 2018: Inverse Cascades of Kinetic Energy as a Source of Intrinsic Variability: A Global OGCM Study. *J. Phys. Oceanogr.*, **48**, 1385–1408.

Sévellec, F. and S. S. Drijfhout, 2019: The Signal-to-Noise Paradox for Interannual Surface Atmospheric Temperature Predictions. *Geophys. Res. Lett.*, **46**, 9031–9041.

Accepted for publication in *Journal of Physical Oceanography*. DOI 10.1175/JPO-D-20-0141.1.

Sévellec, F. and A. V. Fedorov, 2013: The leading, interdecadal eigenmode of the Atlantic meridional overturning circulation in a realistic ocean model. *J. Climate*, **26**, 2160–2183.

Sévellec, F. and T. Huck, 2015: Theoretical investigation of the Atlantic multidecadal oscillation. *J. Phys. Oceanogr.*, **45**, 2189–2208.

Sévellec, F., T. Huck, and M. Ben Jelloul, 2006: On the mechanism of centennial thermohaline oscillations. *J. Mar. Res.*, **64**, 355–392.

Sévellec, F., et al., 2015: Vertical flow in the Southern Ocean estimated from individual moorings. *J. Phys. Oceanogr.*, **45**, 2209–2220.

—, 2019: Observing the Local Emergence of the Southern Ocean Residual-Mean Circulation. *Geophys. Res. Lett.*, **46**, 3862–3870.

Sinha, A. and R. P. Abernathey, 2016: Time Scales of Southern Ocean Eddy Equilibration. *J. Phys. Oceanogr.*, **46**, 2785–2805.

Smith, R. S. and J. M. Gregory, 2009: A study of the sensitivity of ocean overturning circulation and climate to freshwater input in different regions of the North Atlantic. *Geophys. Res. Lett.*, **36**, L15 701.

Taylor, K. E., R. J. Stouffer, and G. A. Meehl, 2012: An overview of CMIP5 and the experiment design. *Bull. of the Amer. Meteor. Soc.*, **93**, 485–498.

Thompson, A. F. and A. C. Naveira Garabato, 2014: Equilibration of the Antarctic Circumpolar Current by Standing Meanders. *J. Phys. Oceanogr.*, **44**, 1811–1828.

Watanabe, M., et al., 2013: Strengthening of ocean heat uptake efficiency associated with the recent climate hiatus. *Geophys. Res. Lett.*, **40**, 3175–3179.

Wunsch, C., 2002: Ocean Observations and the Climate Forecast Problem. *Int. Geophys.*, **83**, 233–245.

Accepted for publication in *Journal of Physical Oceanography*. DOI 10.1175/JPO-D-20-0141.1.

List of Figures

Accepted for publication in *Journal of Physical Oceanography*. DOI 10.1175/JPO-D-20-0141.1.

Accepted for publication in *Journal of Physical Oceanography*. DOI 10.1175/JPO-D-20-0141.1.

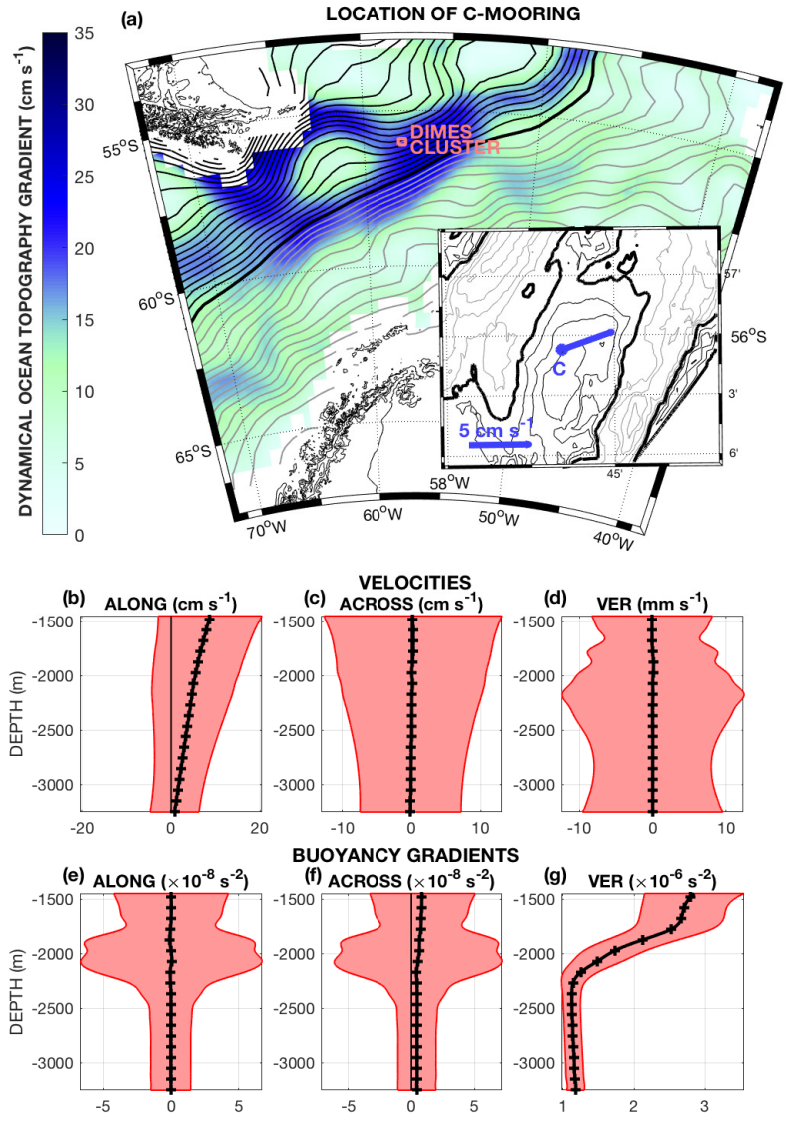

FIGURE 1: (a) Location of the DIMES central mooring, with the red square denoting the location of the 6-mooring cluster. The inset shows a magnification of the region, with the blue circle indicating the central mooring site considered in this study. In the main panel, contours represent the dynamic ocean topography averaged from 1992 to 2002 (Maximenko et al., 2009); the solid thick contour marks −1 m, and solid black and grey contours denote higher and lower values at intervals of 5 cm, respectively. Colour represents the absolute gradient of dynamic ocean topography re-scaled as horizontal geostrophic velocity magnitude. In the inset, the solid thick contours indicate the 4,000 m isobath, and solid black and grey contours denote shallower and deeper isobaths at intervals of 100 m, respectively. The thick blue arrow shows the time- and depth-averaged direction and magnitude of the flow at the mooring location. This average flow direction defines the along direction used in the remainder of our analysis. The across direction is orthogonal to the along direction. (b) Along, (c) across, and (d) vertical velocities, as well as (e) along, (f) across, and (g) vertical buoyancy gradients at the mooring site. Time-mean values are shown on a uniformly spaced 100-m vertical grid (black crosses), connected by a cubic-spline interpolation (black line). The red shading represents plus / minus one temporal standard deviation. Modified from Sévellec et al. (2019).

Accepted for publication in *Journal of Physical Oceanography*. DOI 10.1175/JPO-D-20-0141.1.

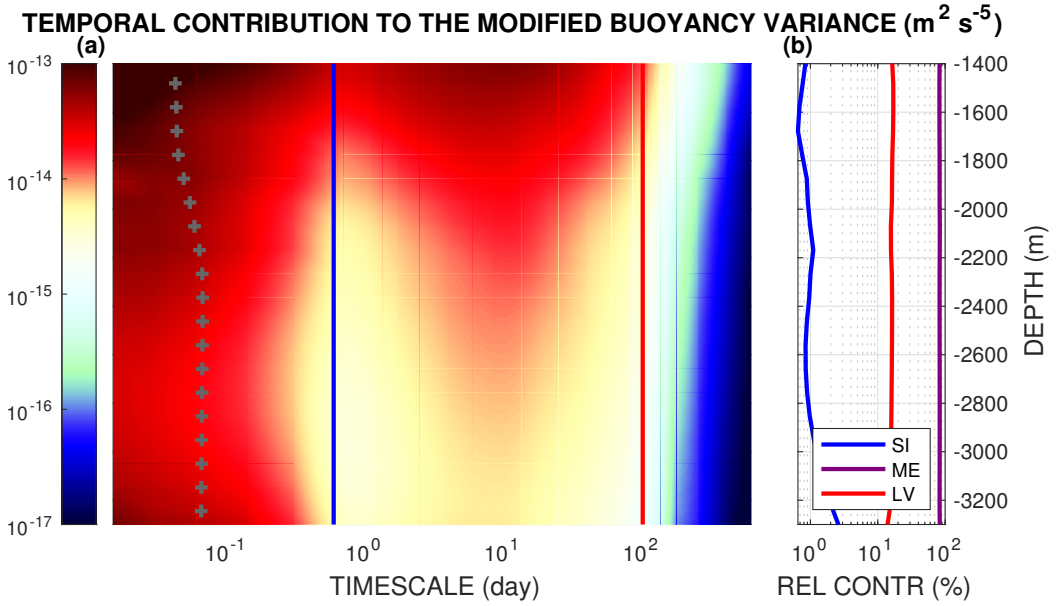

FIGURE 2: (a) Temporal contribution to the total variance of modified buoyancy. This can be related to the power spectral density through Parseval's identity. The vertical blue line represents the inertial period ($2\pi/|f|$, where f is the local Coriolis parameter); the grey crosses mark the internal gravity wave period ($2\pi/N$, where $N^2{=}\partial_z b$ is the time-mean square of the local Brunt-Väisälä frequency); the red vertical line is set at $\tau{=}100$ days and indicates the averaging time scale used in this study to separate short-term fluctuations (mainly driven by mesoscale eddy dynamics) and long-term fluctuations, following previous analyses (Sévellec et al., 2015, 2019). (Note that the horizontal logarithmic scale emphasizes short time scales, despite a weak overall contribution of superinertial motions.) (b) Relative contribution to the total variance of modified buoyancy by superinertial motions (SI, $\tau{<}2\pi/|f|$, blue line), mesoscale eddy fluctuations [ME, $(2\pi/|f|){\geq}\tau{\leq}100$ days, purple line] and long-term variability (LV, $\tau{>}100$ days, red line)

Accepted for publication in *Journal of Physical Oceanography*. DOI 10.1175/JPO-D-20-0141.1.

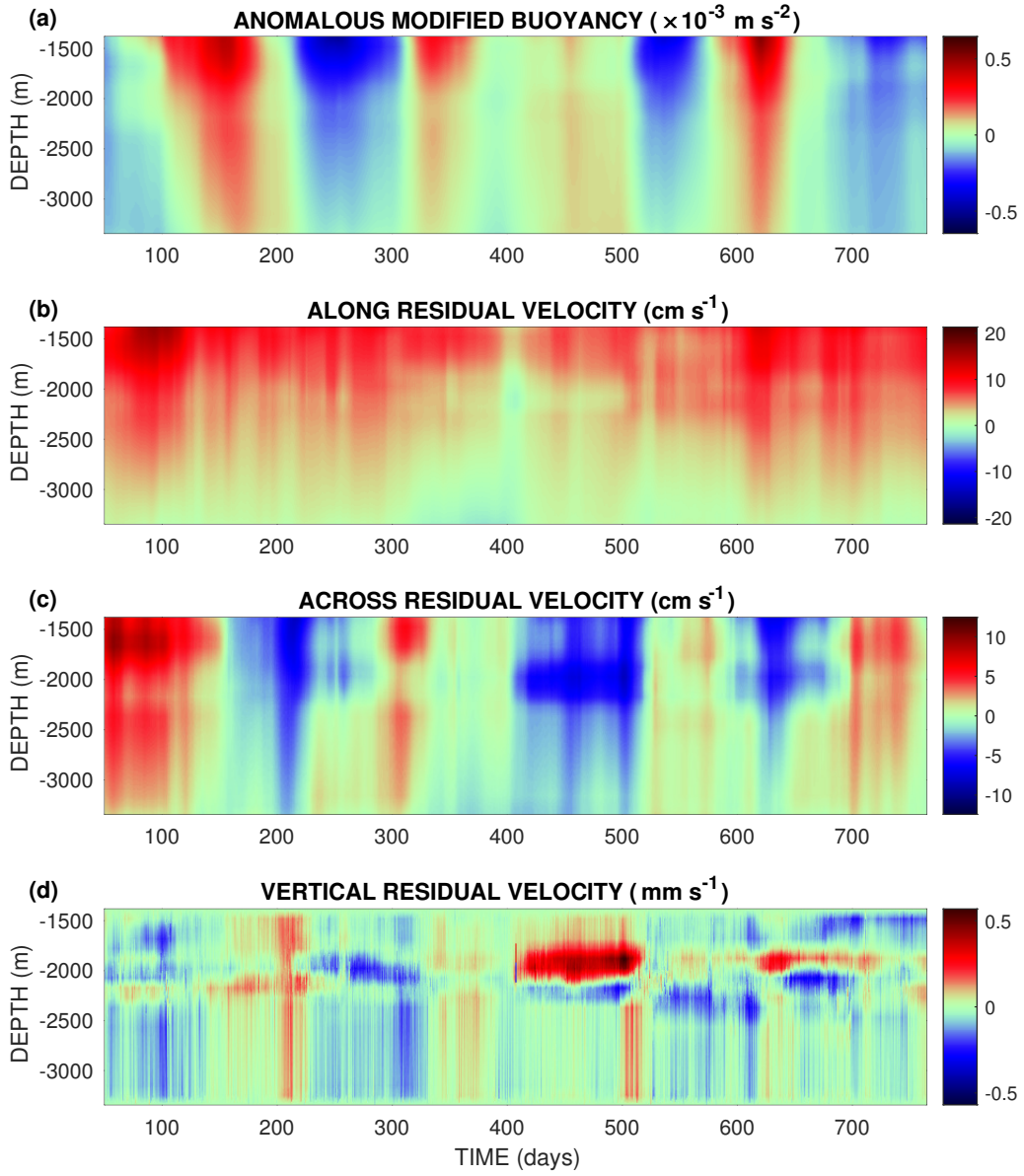

FIGURE 3: (a-d) Hovmöller (time-depth) diagram of the anomalous modified buoyancy (the anomaly is defined in reference to the time-mean modified buoyancy computed at each depth), of the along and across horizontal residual velocities, and of the vertical residual velocity.

Accepted for publication in *Journal of Physical Oceanography*. DOI 10.1175/JPO-D-20-0141.1.

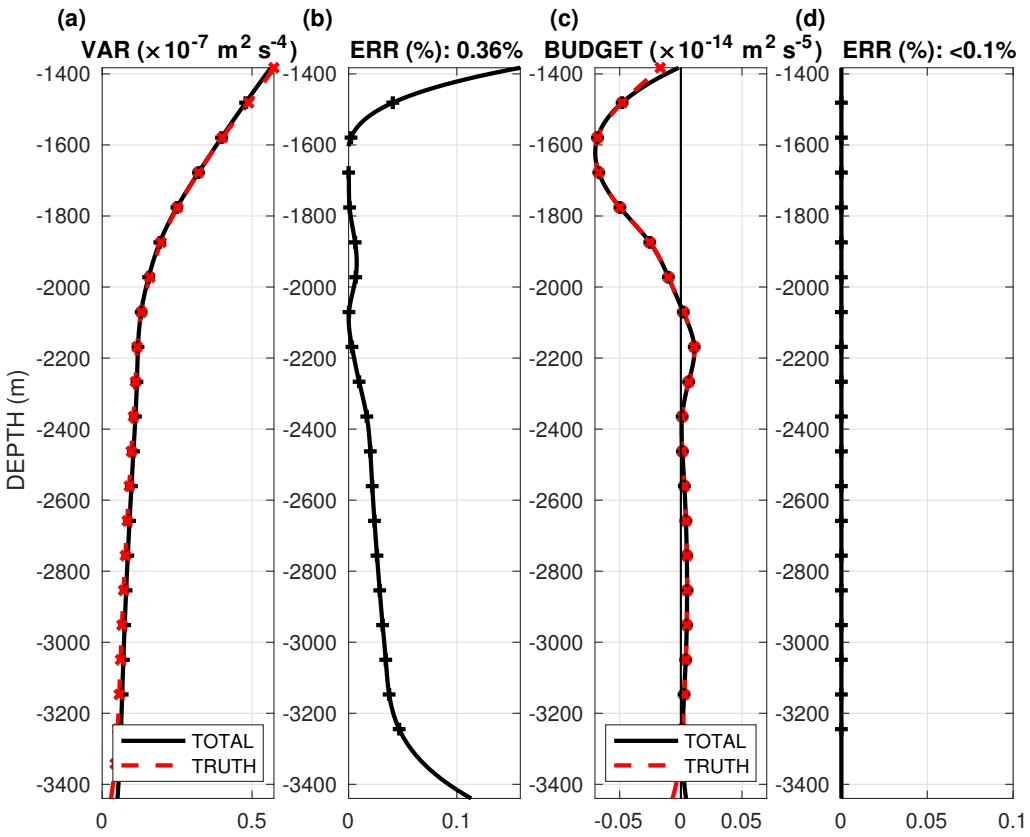

FIGURE 4: (a) Long-term buoyancy variance and (c) long-term variance budget (i.e., 2-yr trend of the long-term buoyancy variance), with relative error of reconstruction after decomposition following (12) and (10) (b and d, respectively). The total cumulative error over the vertical of the variance and its budget are indicated in the title (b and d, respectively). (a and c) Truth (red dashed line) and Total (black solid line) correspond to values computed using the left hand side and sum of the components from right hand side of (12) or (10), respectively. Values are shown on a uniformly spaced 100-m vertical grid (black and red crosses), connected by a cubic-spline interpolation (black solid and red dashed lines).

Accepted for publication in *Journal of Physical Oceanography*. DOI 10.1175/JPO-D-20-0141.1.

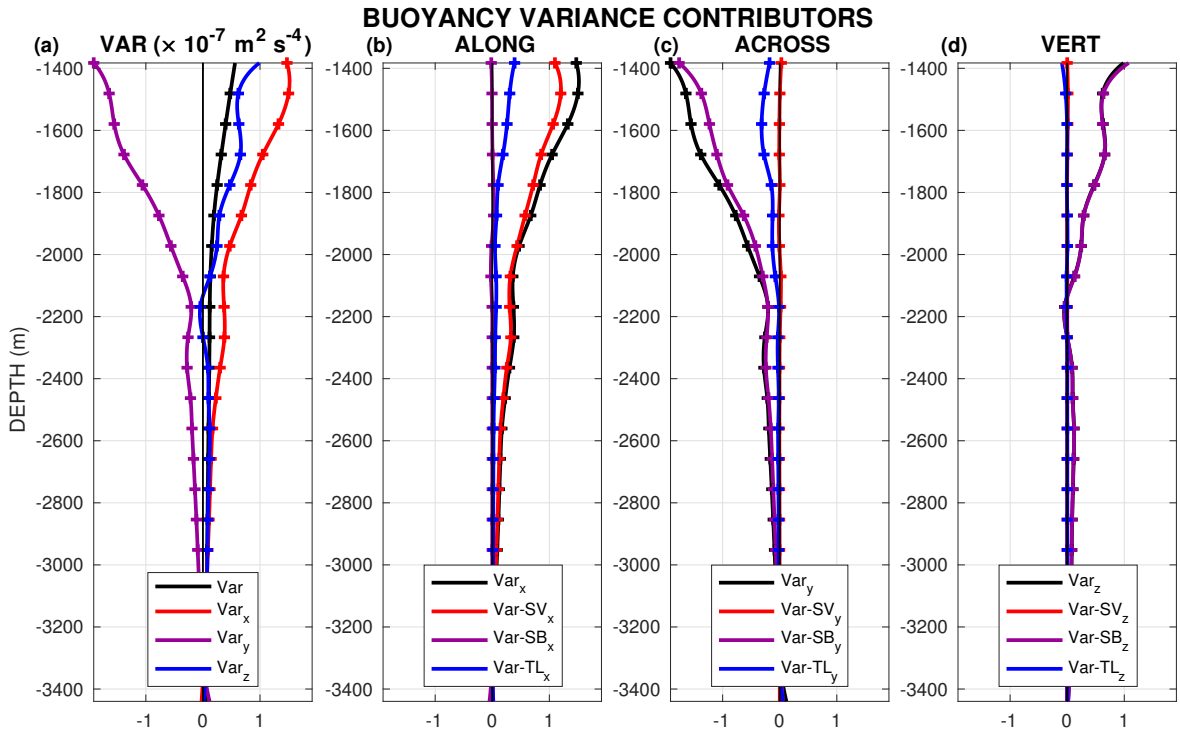

FIGURE 5: Long-term buoyancy variance contributors following (12). The time scale separating short- and long-term fluctuations is set at τ=100 days, such that mesocale dynamics are contained in short-term fluctuations, as shown by Sévellec et al. (2015, 2019) and Fig. 2. Values are shown on a uniformly spaced 100-m vertical grid (crosses), connected by a cubic-spline interpolation (lines).

Accepted for publication in *Journal of Physical Oceanography*. DOI 10.1175/JPO-D-20-0141.1.

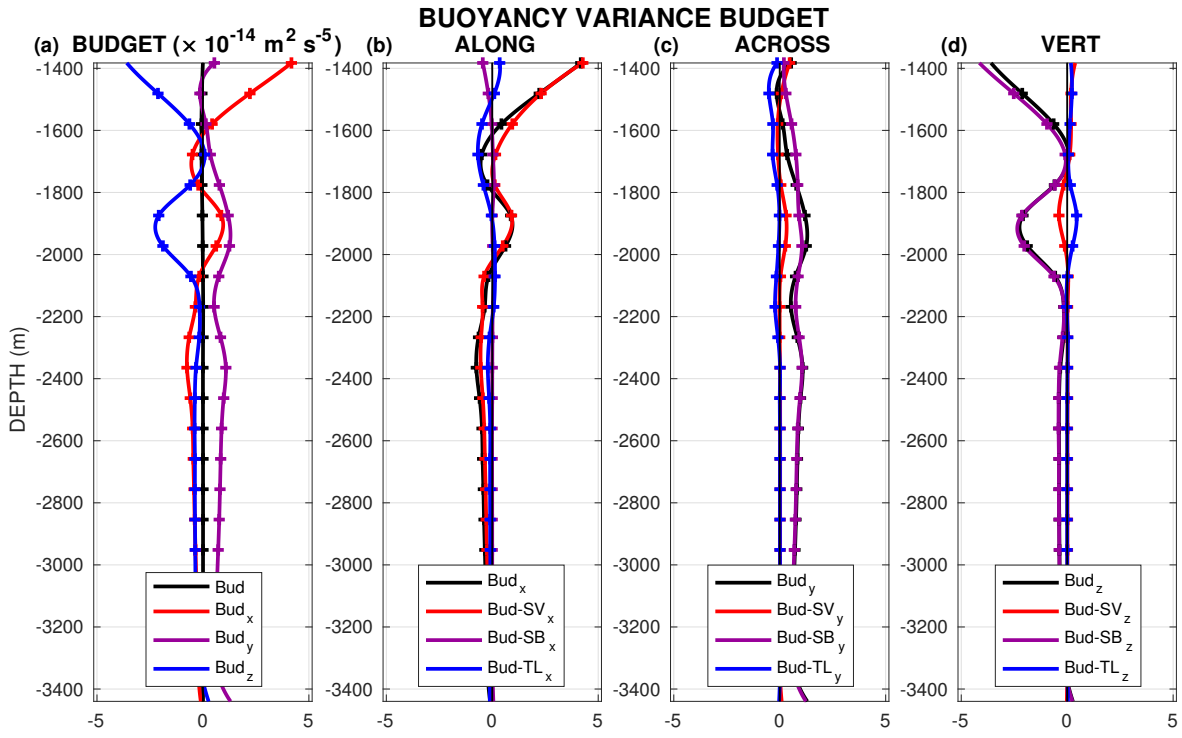

FIGURE 6: Budget of long-term buoyancy variance following (10). The time scale separating short- and long-term fluctuations is set at τ=100 days, such that mesocale dynamics are contained in short-term fluctuations, as shown by Sévellec et al. (2015, 2019) and Fig. 2. Values are shown on a uniformly spaced 100-m vertical grid (crosses), connected by a cubic-spline interpolation (lines).

Accepted for publication in *Journal of Physical Oceanography*. DOI 10.1175/JPO-D-20-0141.1.

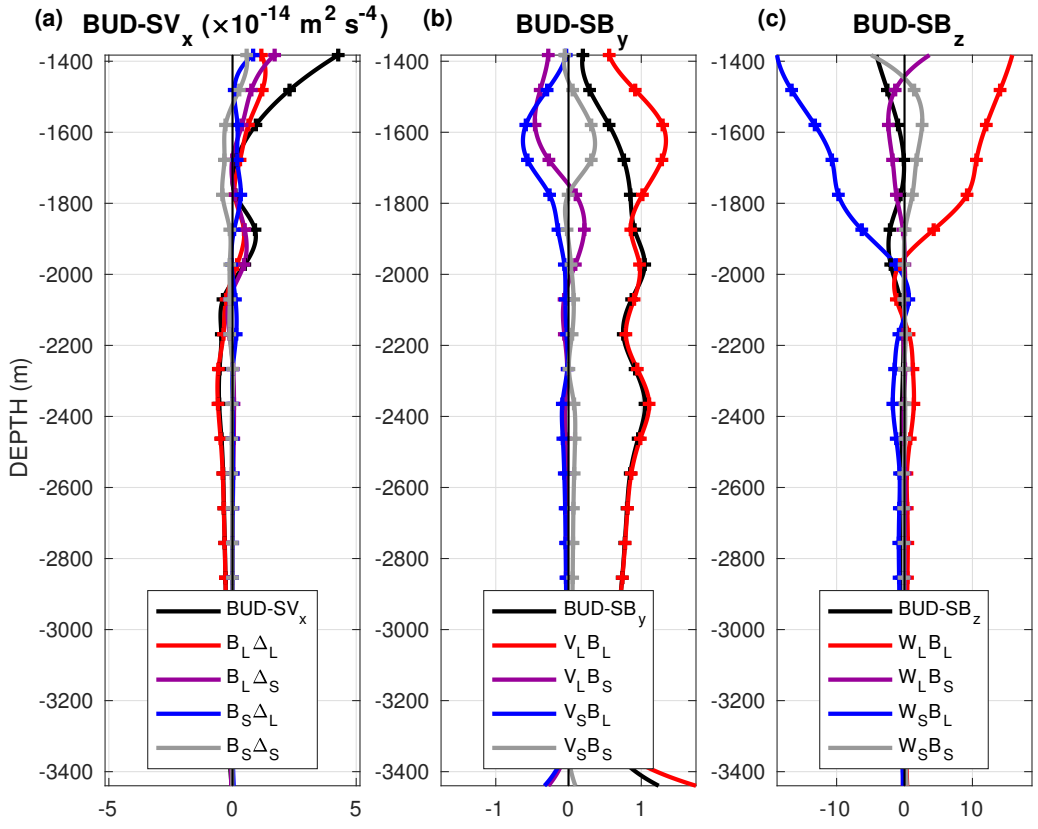

FIGURE 7: Decomposition of the three leading terms in the budget of long-term buoyancy variance following (13). The components in the decomposition are defined in (13). The time scale separating short- and long-term fluctuations is set at τ=100 days, such that mesocale dynamics are contained in short-term fluctuations, as shown by Sévellec et al. (2015, 2019) and Fig. 2. Values are shown on a uniformly spaced 100-m vertical grid (crosses), connected by a cubic-spline interpolation (lines).

Accepted for publication in *Journal of Physical Oceanography*. DOI 10.1175/JPO-D-20-0141.1.

List of Tables

Accepted for publication in *Journal of Physical Oceanography*. DOI 10.1175/JPO-D-20-0141.1.

TABLE 1: Nominal depths of CTD and current meter pairs for the DIMES central mooring used in this study. Data were returned between 12 December 2009 and 6 December 2010, and between 20 December 2010 and 5 March 2012. Full details of the instruments used in each year can be found in the cruise reports (Naveira Garabato, 2010; Meredith, 2011).

Instrument type	Nominal depths (m)
Nortek Acoustic Current Meter	1200, 1299, 1853, 1951, 2049, 2152, 3400, 3600
Seabird Microcat (SMP)	1200, 1299, 1853, 1951, 2049, 2152, 3400, 3600

Accepted for publication in *Journal of Physical Oceanography*. DOI 10.1175/JPO-D-20-0141.1.